J Radioanal Nucl Chem (2013) 297:97–105
DOI 10.1007/s10967-012-2360-3

Removal of U(VI) from aqueous solutions by using attapulgite/iron oxide magnetic nanocomposites

Lei Chen · Jinzhang Xu · Jun Hu

Received: 16 October 2012 / Published online: 11 December 2012

Abstract The attapulgite/iron oxide magnetic nanocomposites were prepared by coprecipitation method and characterized by scanning electron microscopy, X-ray diffraction, vibrating sample magnetometer and Fourier transform infrared sorption spectroscopy. The results of characterization showed that iron oxides were successfully deposited on the surfaces of attapulgite. The prepared magnetic nanocomposites were applied to remove radionuclide U(VI) ions from aqueous solutions by using batch technique and magnetic separation method. The results showed that the sorption of U(VI) on attapulgite/iron oxide magnetic composites was strongly dependent on ionic strength and pH at low pH values, and was independent of ionic strength at high pH values. The interaction of U(VI) with the magnetic nanocomposites was mainly dominated by outer-sphere surface complexation or ion exchange at low pH values, and was controlled by inner-sphere surface complexation or multinuclear surface complexation at high pH values. With increasing temperature, the sorption of U(VI) on attapulgite/iron oxide magnetic composites increased and the thermodynamic parameters calculated from the temperature dependent sorption isotherms suggested that the sorption of U(VI) on the magnetic nanocomposites was a spontaneous and endothermic process. The high sorption capacity and easy magnetic separation of the attapulgite/iron oxide magnetic composites make the material as suitable sorbent in nuclear waste management.

Keywords U(VI) · Attapulgite/iron oxide magnetic nanocomposites · Sorption · Magnetic separation · Ionic strength · pH

L. Chen (✉)
School of Chemical Engineering, Shandong University of Technology, Zibo 255049, Shandong, People's Republic of China
e-mail: chenlei7612@163.com

J. Xu
School of Material Science and Engineering, Hefei University of Technology, Hefei 230031, People's Republic of China

J. Hu
Institute of Plasma Physics, Chinese Academy of Sciences, Hefei 230031, People's Republic of China

Introduction

Uranium(VI), one chemical homolog of long-lived lanthanides and actinides in subsurface environments, has attracted intense interest in multidisciplinary study [1–4]. With the development of nuclear power plants, more and more spent fuels and nuclear waste were generated. In nuclear fuel cycle processes, such as extraction, conversion, enrichment, fabrication and reprocessing, it is inevitable that radioactive U(VI) ions are dispersed into the natural environment. Generally, UO_2^{2+} sorption to clay was strongly dependent on pH values and ionic strength, which suggested that the main sorption mechanism was ion-exchange and/or outer-sphere surface complexation at low pH values, and inner-sphere surface complexation and/or multinuclear surface complexation at high pH values [5–12]. The free radioactive U(VI) ions can directly damage biological organization or produce reactive species (free radicals) that can subsequently react with bio-molecular when human inhales them into body [13]. For example, cancers, including lung cancer, bone cancer, female breast cancer, skin cancer and thyroid cancer, are observed in humans after exposure to radioactive contamination or ionizing radiation. Thereby, in many countries, such as

China, Sweden, Finland, Norway, USA, Canada, India, Iran and Brazil, the problems of groundwater polluted by radionuclides have attracted great attention. WHO recommends the limit of uranium concentration in drinking water below 15 μg/L [14, 15]. Total indicative dose (TID, <0.1 mSv/y) is also used as an additional guidance level for radionuclides in drinking water in many European Union countries [16, 17]. For the sake of public health and environmental pollution, it is necessary to eliminate U(VI) ions from contaminated groundwater as much as possible to the permissible limitation. The sorption of U(VI) on different minerals and oxides have been studied extensively, and the results showed that the interaction mechanism of U(VI) with different materials are quite different, which was dependent on the nature of the sorbent, the species of U(VI) ions and solution chemistry properties etc. [18–26].

Attapulgite, a hydrated magnesium aluminum silicate mineral, consists of two bands of silica tetrahedra linked by magnesium ions in octahedral coordination, and there exist H_2O and exchangeable cations, such as Na^+ and K^+ ions in the repeated units, which can exchange heavy metal ions easily through ion exchange in heavy metal pollution cleanup [27–29]. Attapulgite also has dented surfaces and a relatively high surface area, a moderate cation exchange capacity (CEC), and high acidity. It is important that there are some isomorphic substitutions in the tetrahedral layer, such as Al^{3+} and Si^{4+}, which provide negatively charged adsorption sites to electrostatically adsorb cation ions. From the properties of attapulgite, one can see that attapulgite is a very suitable material for the pre-concentration of heavy metal ions and radionuclides from large volumes of aqueous solutions because of its special structure and surface properties. Fan et al. [27–29] have studied the sorption of radionuclides on attapulgite and found that radionuclides formed strong surface complexes on attapulgite and the attapulgite was a suitable mineral in nuclear waste management. However, the separation of attapulgite from aqueous solution is difficult because of their nanoscale sizes. Although traditional methods such as centrifugation and filtration can be applied to recover the attapulgite particles from aqueous solutions, these methods cannot be applied in large scale in real work. For example, the centrifugation method requires very high centrifugal speed and filtration method is prone to filter blockages. It is necessary to find new method for the separation of attapulgite particles easily and in large scale. Recently, the magnetic separation methods have been widely used and received consideration attention because of their excellent segregative features [30–33]. Although there are a large number of studies on the adsorption of heavy metal ions and radionuclides to magnetic composites, the reports on the adsorption of radionuclides to attapulgite/iron oxide magnetic composites are still not available.

In this paper, we synthesized the attapulgite/iron oxide magnetic nanocomposites by coprecipitation method, and applied the magnetic nanocomposites to remove U(VI) ions from aqueous solutions. The interaction mechanism of U(VI) on the magnetic nanocomposites was discussed from the experimental results.

Experimental

Materials

The attapulgite sample was achieved from Kaidi Co. (Gansu, China). The chemical components analyzed by X-ray fluorescence diffraction are mainly CaO (4.5 %), MgO (6.2 %), Al_2O_3 (15.7 %), SiO_2 (47.0 %), and K_2O (4.0 %) [29]. Prior to the experiments, the attapulgite sample was treated as follows: first dispersion in 5 % hydrochloric acid for 24 h, then the sample was rinsed with Milli-Q water until no chloride was detected in supernatant with 0.01 mol/L $AgNO_3$. Thus achieved sample was dried at 105 °C to eliminate the free water, milled and passed through a 300-mesh screen and used in the experiments.

For the preparation of attapulgite/iron oxide magnetic nanocomposites, positive ferrous and ferric ions are co-precipitated on the surfaces of attapulgite due to the coordination reactions between ferrous and ferric ions and silanol groups (=Si–OH) and aluminol groups (=Al–OH) on attapulgite surfaces. The attapulgite/iron oxide magnetic nanocomposites were prepared from a suspension of 2.0 g attapulgite in 400 mL solution of 11.92 g $FeCl_3{\cdot}6H_2O$ and 6.12 g $FeSO_4{\cdot}7H_2O$ at 70 °C under N_2 atmosphere conditions. NaOH solution (20 mL, 8 mol/L) was added dropwise to precipitate the iron oxides. After the addition of NaOH solution, the mixture was adjusted to pH 11 and stirred for 1 h. The mixture was aged at 70 °C for 4 h and was rinsed with Milli-Q water until the supernatant was neutral. The obtained materials were dried in an oven at 100 °C for 3 h and the derived sample was named as attapulgite/iron oxide magnetic nanocomposites [30]. The relevant chemical reactions can be expressed as follows:

$$Fe^{2+} + 2Fe^{3+} + 8OH^- + \text{attapulgite} \rightarrow \text{attapulgite}/Fe_3O_4 + 4H_2O \quad (1)$$

$$2Fe^{3+} + 5OH^- + \text{attapulgite} \rightarrow \text{attapulgite}/Fe_2O_3 + 2H_2O + H^+ \quad (2)$$

Uranyl stock solution was prepared by dissolving uranyl nitrate hexahydrate ($UO_2(NO_3)_2 \cdot 6H_2O$) in Milli-Q water. The stock solution (8.0×10^{-4} mol/L) was kept at pH 3 and used in the sorption experiments. All chemicals used in the experiments were purchased in analytic purity and used without any purification.

Batch sorption experiments

All sorption experiments were carried out under N_2 conditions by using batch technique. The stock suspension of attapulgite/iron oxide magnetic nanocomposites, $NaClO_4$, and U(VI) stock solution were added in the polyethylene tubes to achieve the desired concentrations of different components. The attapulgite/iron oxide magnetic nanocomposites and $NaClO_4$ were firstly pre-equilibrated for 24 h to achieve the sorption equilibrium of Na^+ with the magnetic nanocomposites, and then the U(VI) stock solution was added into the suspension. The pH of the suspension was adjusted by adding small quantities of 0.1 or 0.01 M $HClO_4$ or NaOH. After the suspensions were shaken for 24 h, the solid and liquid phases were separated by magnetic separation method using a permanent magnet. The concentration of U(VI) was determined by using U Arsenazo-III to form complexes, which can be analyzed by spectrophotometry at the wavelength of 650 nm [10]. The amount of U(VI) adsorbed on attapulgite/iron oxide magnetic nanocomposites was calculated from the difference between the initial concentration and the equilibrium one. The sorption percentage (%) of U(VI) was calculated by the following equation:

$$\text{sorption}\,(\%) = \frac{C_0 - C_{\text{eq}}}{C_0} \times 100\,\% \tag{3}$$

where C_0 (mol/L) is the initial concentration of U(VI) in suspension, and C_{eq} (mol/L) is the equilibration concentration of U(VI) in supernatant after centrifugation.

The distribution coefficient (K_{d}, mL/g) of U(VI) sorption on attapulgite/iron oxide magnetic nanocomposites was calculated using the following equation:

$$K_{\text{d}} = \frac{C_0 - C_{\text{eq}}}{C_{\text{eq}}} \times \frac{V}{m} \tag{4}$$

where V (mL) is the volume of the solution and m (g) is the mass of attapulgite/iron oxide magnetic nanocomposites.

All experimental data were the average of duplicate or triplicate determinations. The relative errors of the data were about 5 %.

Characterization

The surface morphology of attapulgite/iron oxide magnetic nanocomposites was characterized by scanning electron microscopy (SEM). The surface functional groups were characterized by Fourier transforms infrared spectra (FTIR) spectroscopy and the structures were characterized by X-ray diffraction (XRD). The SEM images were obtained at 5.0 kV on a field emission scanning electron microscope (Hitachi S-4800). The FTIR spectrum measurement was performed on a Bruker EQUINOX55 spectrometer (Nexus) in a KBr pellet at room temperature. XRD pattern of the sample was obtained from a D/Max-rB equipped with a rotation anode using Cu Kα radiation ($\lambda = 0.15406$ nm). The XRD device was operated at 40 kV and 80 mA. The measurements were carried out in the range of $5° \leq 2\theta \leq 70°$. The magnetic property was analyzed by the vibrating sample magnetometer analysis. Magnetic curves were obtained using a model 155VSM at room temperature, and its measurement range was 0 to ±12.0 KOe.

Results and discussion

Characterization

Figure 1 shows the SEM images of Na-attapulgite and attapulgite/iron oxide magnetic nanocomposites. One can see that the attapulgite exhibits a fibrous structure and some fibers form straight parallel aggregates. The surface morphology of attapulgite/iron oxide magnetic nanocomposites (Fig. 1b) is obvious difference with that of attapulgite. The magnetic composites show a tighter and rougher surface, which may be attributed to the introduced iron oxides on the surfaces of attapulgite. The SEM images show that the attapulgite/iron oxide magnetic nanocomposites are successfully synthesized.

Figure 2 shows the XRD patterns of attapulgite and attapulgite/iron oxide magnetic nanocomposites. The characteristic peaks at 2θ values of 20.7, 26.6 and 42.5 are observed in the XRD pattern of attapulgite. The peaks at 2θ values of 30.0, 35.4, 36.6, 43.1, 53.4, 57.0 and 62.8 are close to the JCPD standards of Fe_3O_4 or Fe_2O_3 [34, 35]. The quartz and α-FeO(OH) (goethite) are also determined in the XRD patterns, which are also marked in Fig. 2.

Figure 3 shows the FTIR spectra of attapulgite and attapulgite/iron oxide magnetic nanocomposites. The peaks at 3,620 and 3,560 cm^{-1} in attapulgite sample correspond to the stretching vibrations of AlOH and FeOH unites, respectively. The peaks at 1,018 and 474 cm^{-1} are attributed to the Si–O–Si bonds, and the peak at 800 cm^{-1} is attributed to the stretching vibration of Al–O–Si bonds. The peaks at 3,420 and 1,660 cm^{-1} correspond to the bend vibration of zeolite water [36–39]. In the FTIR spectrum of attapulgite/iron oxide magnetic nanocomposites, the peaks at 880 and 790 cm^{-1} correspond to the vibration of Fe–O–Fe bond, which is attributed to the presence of iron oxide in the magnetic composites.

Figure 4 shows the plots of magnetization versus magnetic field for attapulgite and attapulgite/iron oxide magnetic nanocomposites, respectively. The saturation magnetization (Ms) of the magnetic composites is calculated to be 33 emu/g. The bare attapulgite sample has no

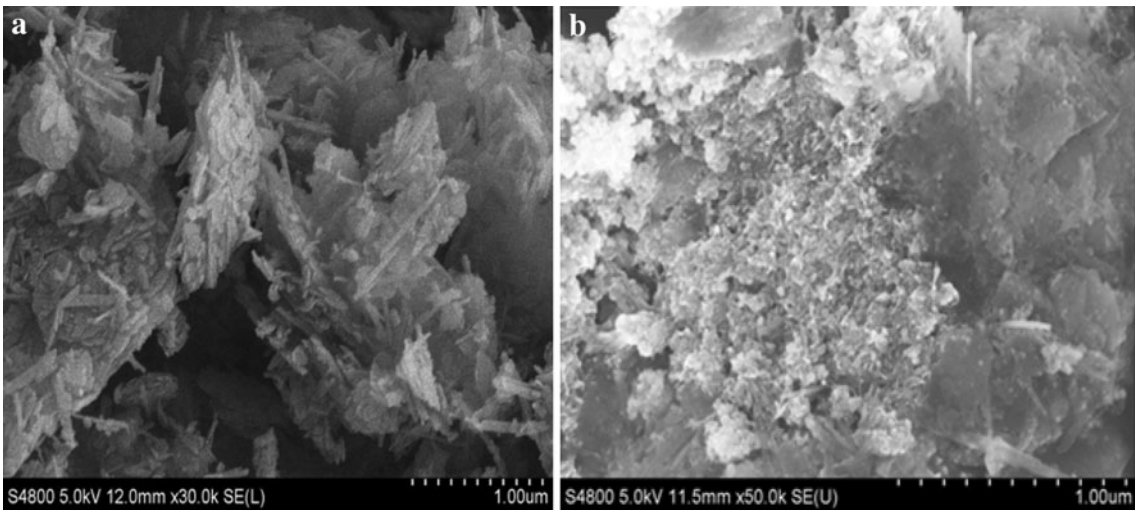

Fig. 1 SEM images of **a** Na-attapulgite and **b** attapulgite/iron oxide magnetic nanocomposites

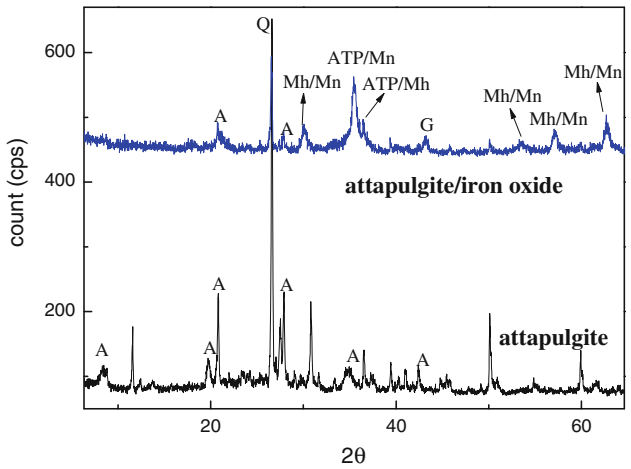

Fig. 2 XRD patterns of attapulgite and attapulgite/iron oxide magnetic nanocomposites. *A* attapulgite, *Q* Quartz, *Mh* maghemite, *Mn* magnetite, G = α-FeO(OH)

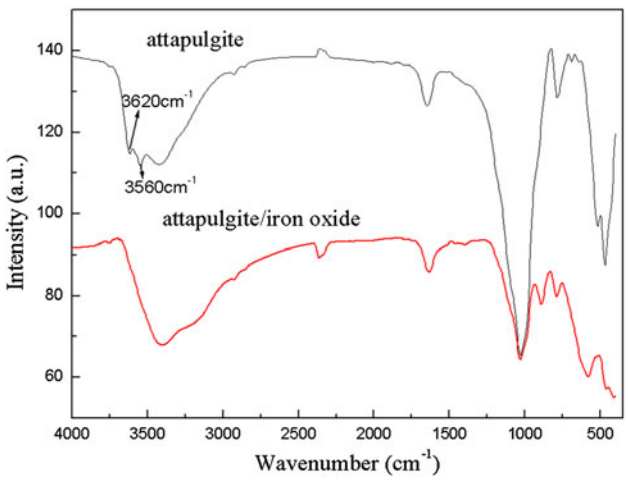

Fig. 3 FTIR spectra of attapulgite and attapulgite/iron oxide magnetic nanocomposite

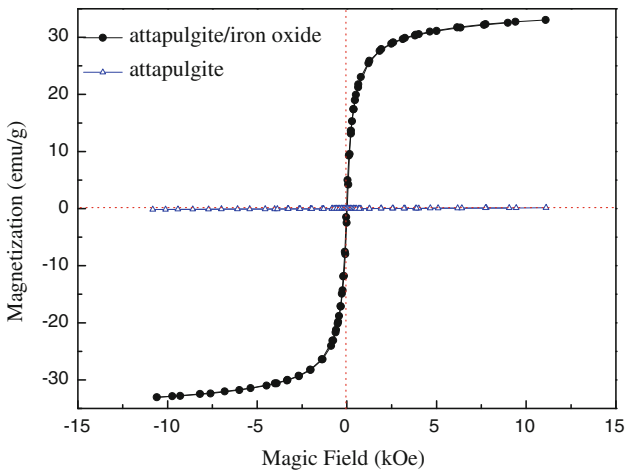

Fig. 4 Magnetization versus magnetic field for attapulgite and attapulgite/iron oxide magnetic nanocomposites

magnetic property. The magnetic property of the magnetic nanocomposites can make them to be separated from aqueous solutions easily from large volumes of aqueous solutions.

Effect of contact time

Sorption of U(VI) on attapulgite/iron oxide magnetic nanocomposites as a function of contact time is shown in Fig. 5. As can be seen from Fig. 5, the sorption of U(VI) on attapulgite/iron oxide magnetic nanocomposites is rapid over the first contact time of 2 h, then slowly and after about 5 h of contact time, the sorption maintains a high level with increasing contact time. The quick sorption of U(VI) on attapulgite/iron oxide magnetic nanocomposites suggests that chemical sorption and/or surface complexation rather

than physical sorption contributes U(VI) sorption on attapulgite/iron oxide magnetic nanocomposites [40–42]. In the following experiments, the shaking time was fixed to 24 h to assure that the sorption of U(VI) on attapulgite/iron oxide magnetic nanocomposites achieves equilibrium.

To analyze the sorption kinetics of U(VI) on attapulgite/iron oxide magnetic nanocomposites, a pseudo-second-order rate equation was applied to simulate the kinetic sorption data [43]:

$$\frac{t}{q_t} = \frac{1}{2K' q_e^2} + \frac{t}{q_e} \quad (5)$$

where q_t (mol/g) is the amount of U(VI) adsorbed on the magnetic nanocomposites at time t (h), and q_e (mol/g) is the equilibrium sorption capacity. K' (g/(mol h)) is the pseudo-second-order rate constant of sorption. A linear plot feature of t/q_t versus t is shown in the inset of Fig. 5. The equilibrium sorption capacity of U(VI) on the magnetic nanocomposites calculated from the slope is 2.81×10^{-5} mol/g. The correlation coefficient of the pseudo-second-order equation for the linear plots is very close to 1, indicating that kinetic sorption is well described by the pseudo-second-order rate model [44].

Effect of ionic strength

Figure 6 shows the effect of $NaClO_4$ concentration on the sorption of U(VI) onto attapulgite/iron oxide magnetic nanocomposites. One can see that the sorption of U(VI) on the magnetic nanocomposites increases with a rise in ionic strength at pH <6, and is independent of ionic strength at pH >6. From the triple-layer model, a possible equilibrium sorption reaction of U(VI) ions with the magnetic nanocomposites can be expressed as follows: (1) If U(VI) ions react similarly to a background electrolyte with the magnetic nanocomposites, then ion-pairs are formed at the β-plane, on which the sorption process is nonspecific and the reaction product is an outer-sphere surface complex; (2) If the sorption of U(VI) ions is visualized as a specific reaction, then the reaction can be considered as an inner-sphere surface coordination process; (3) If hydrate U(VI) ions react with the magnetic nanocomposites and inner-sphere and/or outer-sphere surface complexes can be formed, respectively [45–48].

The concentration of background electrolyte $NaClO_4$ influences the thickness and interface potential of the double layer, affecting the binding of the adsorbed U(VI) species. The background electrolyte ions are placed in the same plane as the outer-sphere surface complexes. Thus outer-sphere surface complexation is expected to be more susceptible to ionic-strength variations than inner-sphere surface complexation [49–51]. Thereby, at pH <6, the sorption of U(VI) on the magnetic nanocomposites are dominated by outer-sphere surface complexation or ion exchange, whereas the sorption of U(VI) is mainly dominated by inner-sphere surface complexation at pH 6. Hayes and Leckie [52] proposed that the influence of the background electrolyte on the sorption reaction can be used to predict the sorption reaction. β-plane sorption can be assumed to proceed when the background electrolyte easily influences the sorption reaction; otherwise, o-plane sorption may occur. From the results, one can conclude that U(VI) sorption is attributed to β-plane complexation at low pH values, affected strongly by ionic strength, which is indicative of the formation of outer-sphere surface complexation [53, 54]. However, U(VI) participates in a

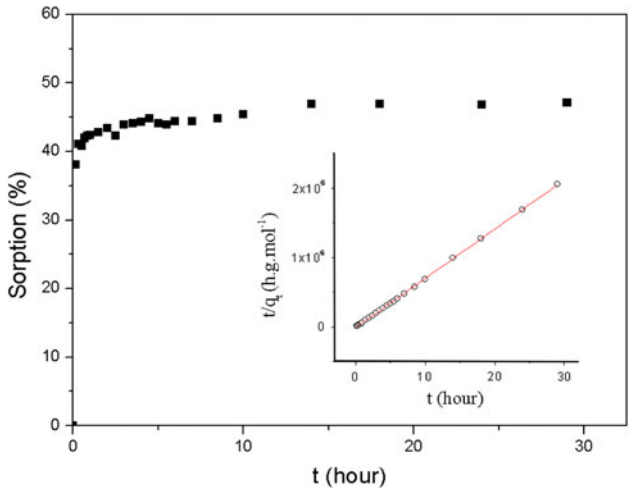

Fig. 5 Effect of contacted time on U(VI) sorption onto attapulgite/iron oxide magnetic nanocomposites. $I = 0.01$ mol/L $NaClO_4$, pH 4.5 ± 0.1, $T = 20$ °C, $m/V = 3$ g/L, $C[U(VI)]_{initial} = 8.0 \times 10^{-5}$mol/L

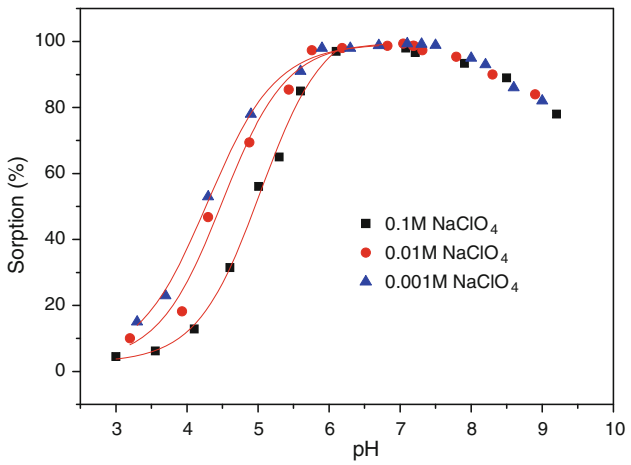

Fig. 6 Effect of pH on U(VI) sorption onto attapulgite/iron oxide magnetic nanocomposites in different $NaClO_4$ concentrations. $T = 20$ °C, $m/V = 3$ g/L, shaking time: 24 h, $C[U(VI)]_{initial} = 8.0 \times 10^{-5}$mol/L

o-plane complex reaction at high pH values, without being affected by the background electrolyte ($NaClO_4$), which is in good agreement with the formation of inner-sphere surface complexes.

At pH >7.5, one can see that the sorption of U(VI) decreases with increasing pH values. This may be attributed to the surface property of the magnetic nanocomposites and the species of U(VI) ions in aqueous solutions at different pH values. In order to properly explain U(VI) sorption behavior, the relative aqueous species of U(VI) as a function of pH was calculated according to the thermodynamic data listed in Table 1 [55, 56]. The distribution of aqueous U(VI) relative species in water solution at U(VI) concentration of 2.0×10^{-5} mol/L is shown in Fig. 7. One can see that the relative distribution of U(VI) species shows a dependency on pH values. Free uranyl ion (UO_2^{2+}) is the dominant species at pH <5, whereas U(VI) hydrolysis complexes and multinuclear hydroxide complexes are the dominant species in U(VI) aqueous solutions. At pH <7.5, U(VI) species are mainly positively charged, and negatively charged at pH >7.5. Thereby, at pH >7.5, the negatively charged U(VI) species are difficult to be adsorbed on the negatively charged surface of magnetic nanocomposites, and thereby results in the decrease of U(VI) sorption on the solid particles.

Sorption isotherms and thermodynamic parameters

Figure 8 shows the sorption isotherms of U(VI) on Fe_3O_4, attapulgite and attapulgite/iron oxide magnetic nanocomposites, respectively. One can see that the sorption isotherm of U(VI) on attapulgite is the highest, and that of U(VI) on Fe_3O_4 is the lowest, suggesting that the pure attapulgite has the highest adsorption capacity in the removal of U(VI) from aqueous solutions. Although the sorption capacity of attapulgite/iron oxide magnetic nanocomposites is a little lower than that of pure attapulgite, the easy magnetic separation of the composites from aqueous solution makes the composites suitable materials from large volumes of aqueous solutions in large scale in real application.

Table 1 Aqueous complexation reactions of U(VI)

Reactions	log K ($I = 0$)
$UO_2^{2+} + H_2O = UO_2(OH)^+ + H^+$	−5.25
$UO_2^{2+} + 2H_2O = UO_2(OH)_2^0 + 2H^+$	−12.15
$UO_2^{2+} + 3H_2O = UO_2(OH)_3^- + 3H^+$	−20.25
$UO_2^{2+} + 4H_2O = UO_2(OH)_4^{2-} + 4H^+$	−32.4
$2UO_2^{2+} + H_2O = (UO_2)_2(OH)^{3+} + H^+$	−2.70
$2UO_2^{2+} + 2H_2O = (UO_2)_2(OH)_2^{2+} + 2H^+$	−5.62
$3UO_2^{2+} + 5H_2O = (UO_2)_3(OH)_5^+ + 5H^+$	−15.55
$3UO_2^{2+} + 7H_2O = (UO_2)_3(OH)_7^- + 7H^+$	−32.20
$4UO_2^{2+} + 7H_2O = (UO_2)_4(OH)_7^+ + 7H^+$	−21.90

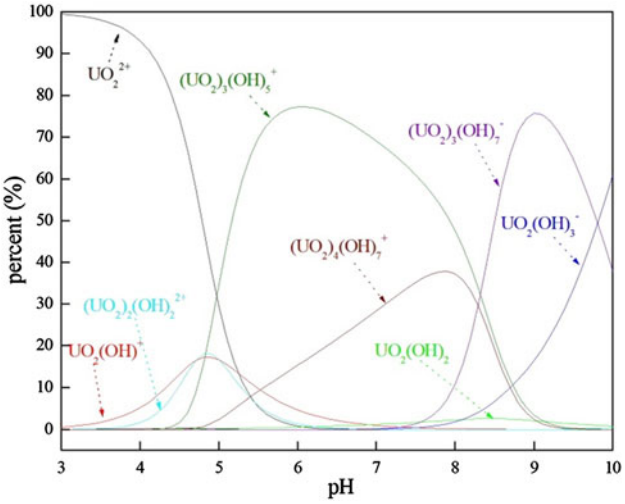

Fig. 7 The relative distribution of aqueous U(VI) species as a function of pH values

In order to simulate the sorption data and to explain the interaction mechanism between U(VI) ions with the solid particles, the experimental data are modeled with the Langmuir and Freundlich model, respectively. The Langmuir model is commonly used to describe the monolayer sorption process. It can be expressed by the following equation [57, 58]:

$$q_e = \frac{bq_{max}C_e}{1 + bC_e} \tag{6}$$

Equation (6) can be expressed in linear form:

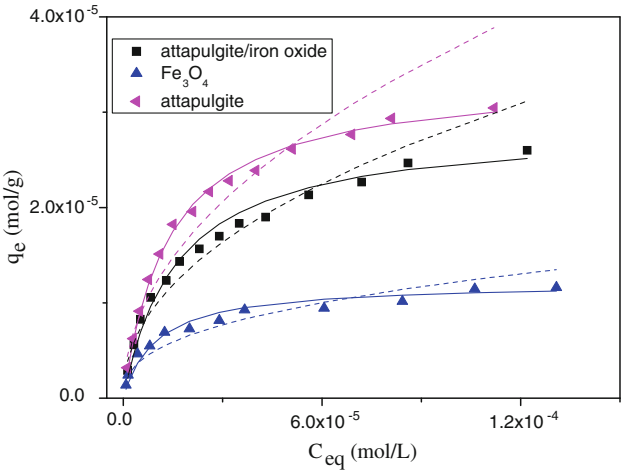

Fig. 8 Sorption isotherms of U(VI) on attapulgite/iron oxide magnetic nanocomposites, attapulgite and Fe_3O_4. $m/V = 3$ g/L, $I = 0.01$ mol/L $NaClO_4$, pH 4.50 ± 0.01. $T = 20 \pm 1$ °C, shaking time: 24 h. *Solid lines* Langmuir model; *Dash lines* Freundlich model

$$\frac{C_e}{q_e} = \frac{1}{bq_{max}} + \frac{C_e}{q_{max}} \quad (7)$$

where C_e is the equilibrium concentration of U(VI) remained in aqueous solution (mol/L); q_e is the amount of U(VI) adsorbed on per weight unit of solid component after sorption equilibration (mol/g); q_{max}, the maximum sorption capacity, is the amount of U(VI) adsorbed at complete monolayer coverage (mol/g), and b (L/mol) is a constant that relates to the heat of sorption.

The Freundlich model represents properly the sorption data at low and intermediate concentrations on heterogeneous surfaces [59]:

$$q_e = k_F C_e^n \quad (8)$$

Equation (8) can be expressed in linear form:

$$\log q_e = \log k_F + n \log C_e \quad (9)$$

where k_F (mol^{1-n} L^n/g) represents the sorption capacity when U(VI) equilibrium concentration equals to 1, and n represents the degree of dependence of sorption with equilibrium concentration.

The sorption isotherms of U(VI) on Fe_3O_4, attapulgite and attapulgite/iron oxide magnetic nanocomposites, are simulated by the Langmuir and Freundlich sorption models, respectively, and the results are also shown in Fig. 8. The relative parameters calculated from the two models are listed in Table 2. From the parameters in Table 2, one can see that the sorption isotherms of U(VI) are better described by the Langmuir model than by the Freundlich model, suggesting that the interaction of U(VI) on the magnetic nanocomposites or on pure attapulgite is a monolayer sorption process [60].

The sorption isotherms of U(VI) on the magnetic nanocomposites at three different temperatures are shown in Fig. 9. The sorption isotherm of U(VI) at $T = 333$ K is the highest and that of U(VI) at $T = 293$ K is the lowest, indicating that the sorption of U(VI) on the attapulgite/iron oxide magnetic nanocomposites is enhanced at high temperatures, and the sorption is an endothermic process. The sorption isotherms are also simulated by Langmuir and Freundlich models, respectively, and the simulation results are also shown in Fig. 9. The relative parameters calculated from the two models are listed in Table 2.

The thermodynamic parameters (ΔG°, ΔS° and ΔH°) for U(VI) sorption on attapulgite/iron oxide magnetic nanocomposites can be calculated from the temperature dependent sorption isotherms. The standard free energy change (ΔG°) can be calculated from the following equation [61]:

$$\Delta G^\circ = -RT \ln K^\circ \quad (10)$$

where R is the universal gas constant (8.314 J/(mol K)), T is the temperature in Kelvin. The sorption equilibrium constant, K°, can be calculated by plotting $\ln K_d$ versus C_{eq} and extrapolating C_{eq} to zero.

The standard enthalpy change (ΔH°) and the standard entropy change (ΔS°) can be calculated according to the following equation [62]:

$$\ln K^\circ = \frac{\Delta S^\circ}{R} - \frac{\Delta H^\circ}{RT} \quad (11)$$

The slope and intercept of the plot of $\ln K^\circ$ versus $1/T$ are $-\Delta H^\circ/R$ and $\Delta S^\circ/R$, respectively (Fig. 10). The thermodynamic data calculated from the sorption isotherms at pH 4.50 and three different temperatures from Eqs. (10) and (11) are tabulated in Table 3. The positive value of ΔH° (9.06 kJ/mol) indicates that the sorption of U(VI) on attapulgite/iron oxide magnetic nanocomposites is an endothermic process. The interpretation to the endothermicity of ΔH° value is that U(VI) ions are well solvated in aqueous solutions. In order to be adsorbed on attapulgite/iron oxide magnetic nanocomposite surfaces, the aqueous U(VI) ions have to be denuded their hydration sheath to some extent, and this dehydration process needs energy [63, 64]. The energy of dehydration exceeds the exothermicity of the U(VI) ions attaching to the surface of the magnetic nanocomposites, and this removal of water molecules from U(VI) ions is an endothermic process, which suggests that the endothermicity of the desolvation process exceeds the enthalpy of U(VI) sorption on the magnetic nanocomposites [65–67]. The positive ΔS° value (87.30 J/(mol K)) also suggests that the sorption is a spontaneous process, which is in good agreement with the negative ΔG° values. It is interesting to notice that the

Table 2 The parameters for Langmuir and Freundlich isotherms for different sorbents and at different temperatures

T (K)	Langmuir			Freundlich		
	q_{max} (mol/g)	b (L/mol)	CC	k_F (mol^{1-n} L^n/g)	n	CC
293 K, Fe_3O_4	1.21×10^{-5}	9.98×10^4	0.990	4.07×10^{-4}	0.381	0.940
293 K, attapulgite	3.37×10^{-5}	7.23×10^4	0.992	3.09×10^{-3}	0.481	0.944
293 K, attapulgite/iron oxide	2.85×10^{-5}	6.15×10^4	0.989	1.95×10^{-3}	0.459	0.938
313 K, attapulgite/iron oxide	4.57×10^{-5}	3.50×10^4	0.997	3.56×10^{-3}	0.495	0.939
333 K, attapulgite/iron oxide	4.81×10^{-5}	4.87×10^4	0.986	4.52×10^{-3}	0.498	0.968

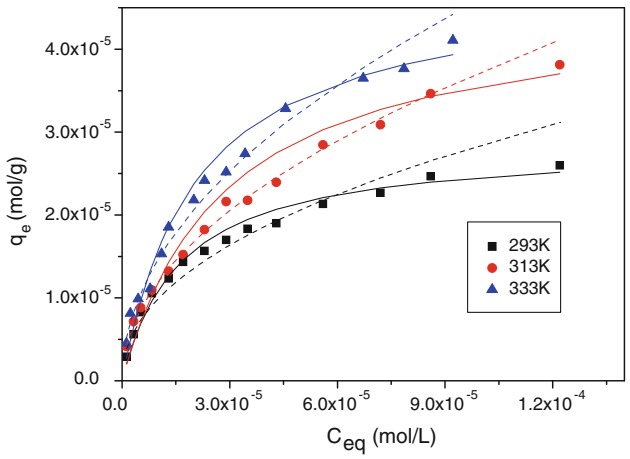

Fig. 9 Sorption isotherms of U(VI) on attapulgite/iron oxide magnetic nanocomposites at different temperatures. $m/V = 3$ g/L, $I = 0.01$ mol/L $NaClO_4$, pH 4.50 ± 0.01. *Solid lines* Langmuir model; *Dash lines* Freundlich model

$\Delta G°$ values decrease with increasing temperature, indicating that the sorption is much higher at higher temperatures. At higher temperature, the U(VI) ions are readily dehydrated, and therefore the sorption of U(VI) to the magnetic nanocomposites becomes more favorable [68]. The thermodynamic data indicates the affinity of the attapulgite/iron oxide magnetic nanocomposites toward U(VI) ions in aqueous solutions and also suggests that some structural changes happen on the magnetic nanocomposites [65, 69].

Conclusion

In this paper, the attapulgite/iron oxide magnetic nanocomposites were synthesized and the characterization indicated that the magnetic iron oxide nanoparticles were successfully precipitated on the surface of attapulgite. The synthesized magnetic nanocomposites were applied as adsorbent for the pre-concentration of U(VI) ions from large volumes of aqueous solutions and the materials could be separated from solution by magnetic separation method easily in large scale. The interaction of U(VI) on the magnetic nanocomposites was dominated by outer-sphere surface complexation or ion exchange at low pH values, and by inner-sphere surface complexation or multinuclear surface complexation at high pH values. The thermodynamic parameters calculated form the temperature dependent sorption isotherms suggested that the sorption of U(VI) on the magnetic nanocomposites was an endothermic and spontaneous process. Although the sorption capacity of the magnetic nanocomposites was a little lower than that of pure attapulgite, the easy separation of the magnetic nanocomposites made this material as suitable candidate in the removal of radionuclides from large volumes of aqueous solutions in large scale in real applications.

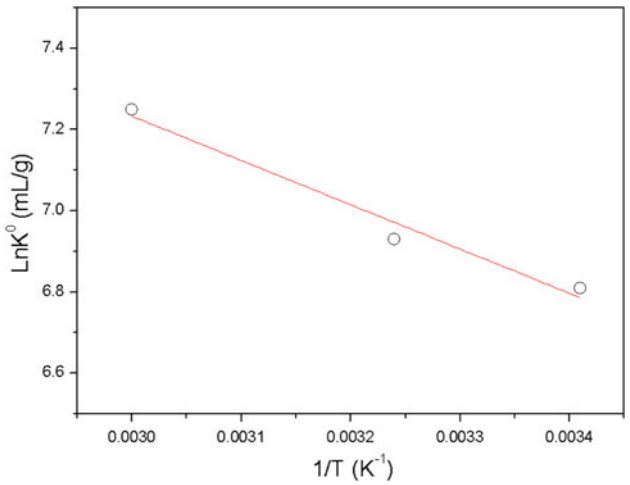

Fig. 10 Linear plots of Ln$K°$ versus $1/T$ for U(VI) sorption on attapulgite/iron oxide magnetic nanocomposites at 293, 313, 333 K. pH 4.50 ± 0.01, C[$NaClO_4$] = 0.01 mol/L, $m/V = 3$ g/L

Table 3 The thermodynamic parameters of U(VI) sorption on attapulgite/iron oxide magnetic nanocomposites

Temperature (K)	$\Delta G°$ (kJ/mol)	$\Delta H°$ (kJ/mol)	$\Delta S°$ (J/(mol K))
293	−16.59	9.06	87.30
313	−18.03		
333	−20.07		

Acknowledgments Financial supports from National Natural Science Foundation of China (21107115) and Doctoral Fund of Ministry of Education of China (20110111110002) are acknowledged.

References

1. Wang X, Chen C, Zhou X, Tan X, Hu W (2005) Radiochim Acta 93:273
2. Sun Y, Yang S, Sheng G, Guo Z, Tan X, Xu J, Wang X (2011) Sep Purif Technol 83:196
3. Zhao G, Wen T, Yang X, Yang S, Liao J, Hu J, Shao D, Wang X (2012) Dalton Trans 41:6182
4. Ren XM, Wang SW, Yang ST, Li JX (2010) J Radioanal Nucl Chem 283:253
5. Hu J, Shao DD, Chen CL, Sheng GD, Li JX, Wang XK, Nagatsu M (2010) J Phys Chem B 114:6779
6. Wang XK, Chen CL, Hu WP, Ding AP, Xu D, Zhou X (2005) Environ Sci Technol 39:2856
7. Singh A, Ulrich KU, Giammar DE (2010) Geochim Cosmochim Acta 74:6324
8. Stewart BD, Mayes MA, Fendorf S (2010) Environ Sci Technol 44:928
9. Shao DD, Fan QH, Li JX, Niu ZW, Wu WS, Chen YX, Wang XK (2009) Microporous Mesoporous Mater 123:1
10. Shao DD, Jiang ZQ, Wang XK, Li JX, Meng YD (2009) J Phys Chem B 113:860

11. Wang XK, Chen CL, Du JZ, Tan XL, Xu D, Yu SM (2005) Environ Sci Technol 39:7084
12. Yang SB, Hu J, Chen CL, Shao DD, Wang XK (2011) Environ Sci Technol 45:3621
13. Sun YB, Wang Q, Tan XL, Wang XK (2012) Environ Sci Technol 46:6020
14. WHO (2004) Uranium in drinking water. Background document for the development of WHO guidelines for drinking water quality. WHO/SDE/WSH, 03:118
15. Kowal-Fouchard A, Drot R, Simoni E, Ehrhardt JJ (2004) Environ Sci Technol 38:1399
16. Zamora ML, Tracy BL, Zielinski JM, Meyerhof DP, Moss MA (1998) Toxicol Sci 43:68
17. Xu D, Shao DD, Chen CL, Ren AP, Wang XK (2006) Radiochim Acta 94:97
18. Sun YB, Wang Q, Yang ST, Sheng GD, Guo ZQ (2011) J Radioanal Nucl Chem 290:643
19. Zhao DL, Yang SB, Chen SH, Guo ZQ, Yang X (2011) J Radioanal Nucl Chem 287:557
20. Wieland E, Mace N, Dahn R, Kunz D, Tits J (2010) J Radioanal Nucl Chem 286:793
21. Kim JH, Lee HI, Yeon JW, Jung Y, Kim JM (2010) J Radioanal Nucl Chem 286:129
22. Das D, Sureshkumar MK, Koley S, Mithal N, Pillai CGS (2010) J Radioanal Nucl Chem 285:447
23. Ayata S, Aydinci S, Merdivan M, Binzet G, Kulcu N (2010) J Radioanal Nucl Chem 285:525
24. Yusan S, Aslani MAA, Turkozu DA, Aycan HA, Aytas S, Akyil S (2010) J Radioanal Nucl Chem 283:231
25. Wang MM, Qiu J, Tao XQ, Wu CP, Cui WB, Liu Q, Lu SS (2011) J Radioanal Nucl Chem 288:895
26. Humelnicu D, Drochioiu G, Sturza MI, Cecal A, Popa K (2006) J Radioanal Nucl Chem 270:637
27. Fan Q, Shao D, Hu J, Wu W, Wang X (2008) Surf Sci 602:778
28. Fan Q, Shao D, Wu W, Wang X (2009) Chem Eng J 150:188
29. Fan QH, Tan XL, LI JX, Wang XK, Wu WS (2009) Environ Sci Technol 43:3115
30. Chen C, Wang X, Nagatsu M (2009) Environ Sci Technol 43:2362
31. Chen CL, Hu J, Shao DD, Li JX, Wang XK (2009) J Hazard Mater 164:923
32. Wu X, Wang L, Chen C, Xu A, Wang X (2011) J Mater Chem 21:17353
33. Zhao GX, Li JX, Ren XM, Chen CL, Wang XK (2011) Environ Sci Technol 45:10454
34. Hu J, Xu D, Chen L, Wang XK (2009) J Radioanal Nucl Chem 279:701
35. Yang ST, Sheng GD, Tan XL, Hu J, Du JZ, Montavon G, Wang XK (2011) Geochim Cosmochim Acta 75:6520
36. Shao DD, Hu J, Sheng GD, Ren XM, Chen CL, Wang XK (2010) J Phys Chem C 114:21524
37. Sheng GD, Yang ST, Sheng J, Hu J, Tan XL, Wang XK (2011) Environ Sci Technol 45:7718
38. Tan X, Wang X, Geckeis H, Rabung T (2008) Environ Sci Technol 42:6532
39. Zhao GX, Zhang HX, Fan QH, Ren XM, Li JX, Chen YX, Wang XK (2010) J Hazard Mater 173:661
40. Sheng GD, Sheng J, Yang ST, Hu J, Wang XK (2011) J Radioanal Nucl Chem 289:129
41. Wang X, Zhou X, Du J, Hu W, Chen C, Chen Y (2006) Surf Sci 600:478
42. Liu MC, Chen CL, Hu J, Wu XL, Wang XK (2011) J Phys Chem C 115:25234
43. Ho YS, McKay G (1998) Process Saf Environ Prot 76:183
44. Zhao GX, Wen T, Chen CL, Wang XK (2012) RSC Adv 2:9286
45. Wu CH (2007) J Colloid Interface Sci 311:338
46. Xu D, Wang XK, Chen CL, Zhou X, Tan XL (2006) Radiochim Acta 94:429
47. Yang ST, Sheng GD, Guo ZQ, Tan XL, Xu JZ, Wang XK (2012) Sci China Chem 55:632
48. Tan XL, Fan QH, Wang XK, Grambow B (2009) Environ Sci Technol 43:3115
49. Chen C, Wang X (2007) Appl Geochem 22:436
50. Tan XL, Hu J, Zhou X, Yu SM, Wang XK (2008) Radiochim Acta 96:487
51. Chen CL, Hu J, Xu D, Tan XL, Meng YD, Wang XK (2008) J Colloid Interface Sci 323:33
52. Hayes KF, Leckie JO (1987) J Colloid Interface Sci 115:564
53. Sheng GD, Yang ST, Zhao DL, Sheng J, Wang XK (2012) Sci China Chem 55:182
54. Hu J, Xie Z, He B, Sheng GD, Chen CL, Li JX, Chen YX, Wang XK (2010) Sci China Chem 53:1420
55. Bhattacharyya KG, Gupta SS (2008) Colloids Surf A 317:71
56. Shao DD, Hu J, Wang XK (2010) Plasma Process Polym 7:977
57. Zhao GX, Jiang L, He YD, Li JX, Dong HL, Wang XK, Hu WP (2011) Adv Mater 23:3959
58. Shao DD, Xu D, Wang SW, Fan QH, Wu WS, Dong YH, Wang XK (2009) Sci China Chem 52:362
59. Sheng GD, Li JX, Shao DD, Hu J, Chen CL, Chen YX, Wang XK (2010) J Hazard Mater 178:333
60. Yang ST, Li JX, Shao DD, Hu J, Wang XK (2009) J Hazard Mater 166:109
61. Zhao GX, Ren XM, Gao X, Tan XL, Li JX, Chen CL, Huang YY, Wang XK (2011) Dalton Trans 40:10945
62. Ren XM, Yang ST, Tan XL, Chen CL, Wang XK (2012) Sci China Chem 55:1752
63. Zhao GX, Li JX, Wang XK (2011) Chem Eng J 173:185
64. Sun YB, Chen CL, Tan XL, Shao DD, Li JX, Zhao GX, Yang SB, Wang Q, Wang XK (2012) Dalton Trans 41:13388
65. Chen CL, Wang XK (2006) Ind Eng Chem Res 45:9144
66. Tan XL, Hu J, Montavon G, Wang XK (2011) Dalton Trans 40:10953
67. Chen L, Gao B, Lu SS, Dong YH (2011) J Radioanal Nucl Chem 288:851
68. Lv K, Zhao G, Wang X (2012) Chin Sci Bull 57:1223
69. Li J, Zhang S, Chen C, Yang X, Li J, Wang X (2012) ACS Appl Mater Interface 4:4991